DOI: 10.1111/mice.12950

INDUSTRIAL APPLICATION

COMPUTER-AIDED CIVIL AND INFRASTRUCTURE ENGINEERING WILEY

Infrastructure-level traffic micro-simulation for probabilistic analysis of bridge loads

Giusiana Testa[1] | **Gaetano Zaccaria**[2] | **Marcello Montanino**[2] | **Georgios Baltzopoulos**[1] | **Antonio Bilotta**[1] | **Iunio Iervolino**[1] | **Vincenzo Punzo**[2]

[1]Dipartimento di Strutture per l'Ingegneria e l'Architettura, Università degli Studi di Napoli Federico II, Naples, Italy

[2]Dipartimento di Ingegneria Civile e Ambientale, Università degli Studi di Napoli Federico II, Naples, Italy

Correspondence
Iunio Iervolino, via Claudio 21, 80125, Naples, Italy.
Email: iunio.iervolino@unina.it

Funding information
Tangenziale di Napoli s.p.a.–Dipartimento di Strutture per l'Ingegneria e l'Architettura 2021 agreement

Abstract

In state-of-the-art building codes, the traffic loads for the design or assessment of bridges should derive from a probabilistic characterization. However, because traffic depends on the vehicle flow peculiar to the transportation infrastructure of interest, the frequency of exceedance of code-assigned loads is factually unknown. This study presents a methodology to probabilistically characterize the traffic loads on bridges based on network-level traffic micro-simulation and its application to the A56, that is, the urban highway connecting Naples' (Italy) districts. One year of traffic simulations, in conjunction with structural modeling of the bridges featured in the infrastructure, enabled the probabilistic characterization of the traffic-induced structural demand and the determination of the bridge-specific safety margins along the highway. The results of the study and of the application to A56 ultimately show that: (i) traffic micro-simulation appears to be a suitable approach to bridge-specific structural safety assessment; (ii) structural actions deriving from code-assigned loads tend to be conservative with respect to their traffic-simulation-derived counterparts; and (iii) structural demand induced by traffic loads can vary along the same transportation infrastructure.

1 | INTRODUCTION

In state-of-the-art structural codes, traffic loads for the assessment of the safety level of existing bridges are typically based on a semi-probabilistic approach (O'Brien et al., 2015; Wiśniewski et al., 2012). In this framework, the exceedance probability of the structural actions, that is, the effect of these loads, is controlled for any time interval of interest, at least in principle. On the other hand, it is expected that the actual probability according to which the code-prescribed traffic effect is exceeded on a specific bridge in a time interval (or, equivalently, the exceedance *return period,* T_r), depends on the characterization of the traffic on the transportation network to which the bridge belongs (Enright et al., 2013).

Structure-specific traffic load analysis is desirable to determine the safety margin under which the bridge operates and to introduce traffic control measures or structural retrofitting actions if needed. Currently, this is especially relevant in Italy, where strict rules about the operability of road bridges are enforced, based on conventional structural safety checks (C.S.LL.PP., 2020), hereafter DM2020.

When direct traffic observations are not available (Zhang et al., 2019), simulation can be adopted to determine a surrogate of detailed structure-specific traffic data (Olstam & Tapani, 2011). More specifically, traffic micro-simulation is fit for purpose, leading to register the motion of each vehicle along the road featuring the bridge, which—in turn—enables subsequent evaluation of the effects of such traffic. This can be regarded as a progress over earlier concerted efforts to define traffic effects on bridges (Mathieu et al., 1991). In fact, several studies on traffic micro-simulation have been carried out during the last two decades, both for providing a congestion feature extraction model to simulate highway traffic flow (Adeli & Ghosh-Dastidar, 2004; Ghosh-Dastidar & Adeli, 2006) and to show general methodologies to build a traffic flow forecast model (Jiang & Adeli, 2004; Treiber et al., 2011), as well as to localize the effects of disruptive incidents (Karim & Adeli, 2002). Moreover, software has been developed for the evaluation of permit applications for special transits (Waheed & Adeli, 2000) or to support the assessment of existing bridges (Sirca & Adeli, 2005). Nevertheless, transportation engineering models have, so far, yet to be combined with structural models to develop a procedure for transportation-network-specific safety assessment of bridges.

Traffic micro-simulation requires a significant effort in modeling the network's demand–supply interaction—from a transportation engineering point of view—especially concerning the characterization of highly uncertain traffic flows (Buisson et al., 2014; Ciuffo et al., 2008). At the same time, coherent structural modeling is required to translate vehicular traffic into structural actions and safety checks. Both efforts are deemed critical for the defensibility of the results, which is indispensable when structural safety is concerned.

In this context, as a proof-of-concept, this study addresses a traffic analysis via micro-simulation of the A56 *Tangenziale di Napoli*—which is a 20-km urban highway connecting Naples' districts (Italy)—to determine bridge-specific frequentist distributions of traffic loads and the consequent safety margins for some featured bridges, via the characterization of the traffic flows over an entire year of operations. To this aim, a methodology has been developed to estimate a probabilistic model of hourly origin/destination (OD) demand matrices, based on the observed spatial and temporal correlations of available traffic counts. The more than 8000 estimated hourly demand matrices, which constitute a synthetic but representative year of demand data, describing within-day, day-to-day, and seasonal demand variability, have been propagated into the road network via micro-simulation. The individual space–time trajectory of any simulated vehicle (around a total of 8 million vehicles) has allowed us to map vehicle axles, and therefore loads, on any bridge in any instant over one sampled year of traffic operations. Applying such loading schemes to the structural model of each bridge has enabled us to determine the yearly frequency distribution of maximum structural actions (e.g., in terms of internal forces). These distributions have been used to compare the safety margins for some of the bridges of A56, featuring different structural characteristics and located in different sections of the network.

The remainder of the paper is structured so that the methodology developed is presented first. Second, the transportation infrastructure case study is described in the aspects relevant to the analysis. Then, the yearly traffic model and its calibration is discussed, followed by a summary of the simulation results. Subsequently, the structural loading schemes are derived from the traffic simulated on the bridges. The structural models are introduced to derive the load effects and to compare them with those obtained by the application of conventional code-mandated loads, for different operability conditions. Some final remarks conclude the article.

2 | STUDY WORKFLOW

The main output of the analysis is the annual distribution of maximum structural internal forces in the bridges of the A56 highway. This output can be used to get results having a twofold impact: (i) to show that it is possible to probabilistically frame the code-based traffic loads via network-specific micro-simulation; (ii) to carry out a structural safety assessment of the simulated network's bridges with a refined (i.e., network-specific) characterization of uncertainty on traffic loads, with respect to the conventional building code-based provisions. Although this concept has been preliminarily discussed in the literature (Caprani et al., 2016; Lipari et al., 2012), to the authors' knowledge, the presented study in which micro-simulations are used to determine structural loads involving an entire real-case transportation network, is the first of its kind. Since a traffic flow on any specific bridge or stretch of highway is the result of a dynamic combination of time-varying OD travel demand flows, simulating OD flows of a closed network requires to reconstruct vehicle density and distribution over each bridge or other segment, unless temporal inflows and outflows for that bridge/segment are monitored (even in this case, to calculate the vehicle density over a bridge/link as the difference of cumulated inflows and outflows data can be affected by the accumulation of detection errors).

To get the yearly frequency distribution of structural actions on the network's bridges, an articulated methodology, consisting of two main parts, has been followed (see

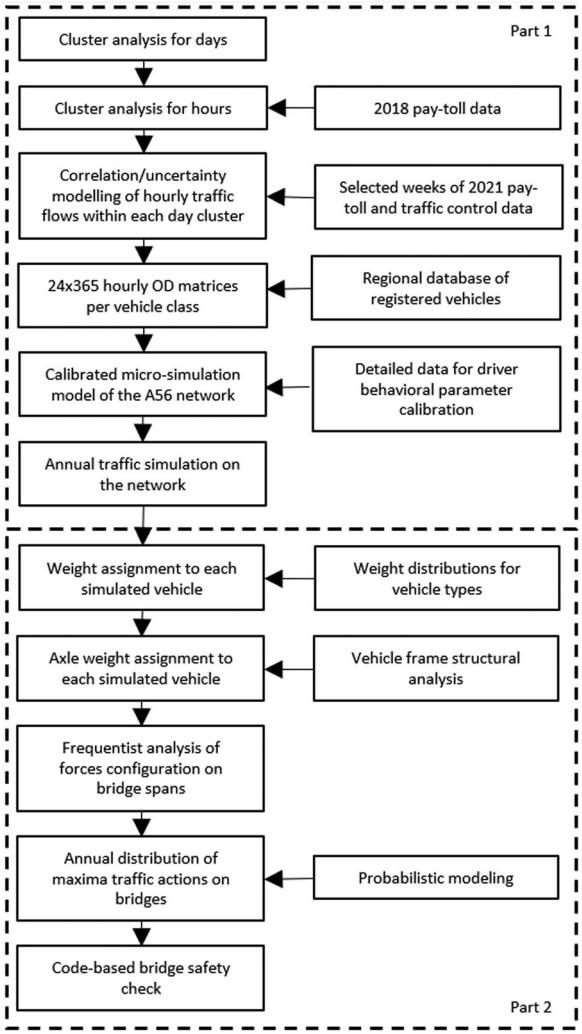

FIGURE 1 Flowchart of the adopted methodology

Figure 1). The first part belongs to the field of transportation engineering, and it is mainly devoted to modeling the daily demand–supply scenarios for the network of interest. This part culminates in simulating the traffic over the network for 1 year. The simulation output consists of the time–space trajectory of any specific vehicle circulating on the A56 in the simulated year. More specifically, the steps leading to traffic simulation develop as follows.

One year (i.e., prepandemic 2018) of detector data was acquired from the network's operator (i.e., Tangenziale di Napoli s.p.a.). The data consist of detector counts at all exit junctions (from toll booths), in addition to mainstream counts from the point-to-point (P2P) speed enforcement system.

Traffic flow data are used in a cluster analysis to identify typical days in 1 year, that is, days where the OD matrices for the network show similar characteristics. Once the clusters have been identified and typical days are defined, a second-level cluster analysis is performed to find whether multiple hours in the same day show similar characteristics within the day; that is, to identify hourly clustering. The cluster data are also used to characterize the hour-to-hour and day-to-day variability (hereafter referred to as *uncertainty*) of traffic flows (Punzo & Montanino, 2020; Rafati Fard & Shariat Mohaymany, 2019), which, in turn, is at the basis of the estimation of hour-specific OD matrices for each day of an entire year.

The OD matrices provide the travel demand in terms of the total number of vehicles originating from a specific origin and moving toward a specific destination of the network, in a specific 1-h interval. The OD flows can be divided in terms of vehicle classes (to follow) using both toll data and vehicle registration data. Individual behavioral parameters of drivers within each class also need to be calibrated.

With this information, the traffic on the network can be simulated for 1 year. The output consists of individual vehicle trajectories, that is, velocity and position of each vehicle in the network at any simulation step, which is 0.1 s.

The second part of the analysis belongs to the structural engineering field and mainly deals with transforming the simulation output into bridge loads, which ends with the safety analysis of the structures. The most relevant effort is the determination of vehicle axle forces acting on the bridges, the bridges' structural modeling, and the probabilistic analysis of traffic-induced structural actions. More specifically, this second part involves the following steps.

Each vehicle is assigned a total weight by sampling frequentist distributions from the literature (Grakovski et al., 2020) for specific typologies of vehicles (this step could be better informed by network-specific data such as *weigh-in-motion* or WIM systems, if available).

A structural analysis, specific to each vehicle type and based on the static scheme of its frame, is used to distribute the total weight to each axle. This enables the transformation of vehicle trajectories obtained from the simulation into trajectories of vertical forces.

A structural model is then developed for some of the network's bridges, based on specific information provided by the network operator. The bridges' structural models are used to determine the internal forces in the critical cross-sections of each bridge deck, produced by each recorded disposition of forces from the previous step, considering only their static effects (for simplicity). Subsequently, these data are used to fit probabilistic models of annual maximum actions on the bridge. These models enable the determination of the annual exceedance frequency for each action, based on the traffic simulations.

Specific quantiles from the fitted distributions are used in conjunction with the other loads acting on the structure to perform safety checks on the bridges in a code-compliant format and to compare against the safety checks

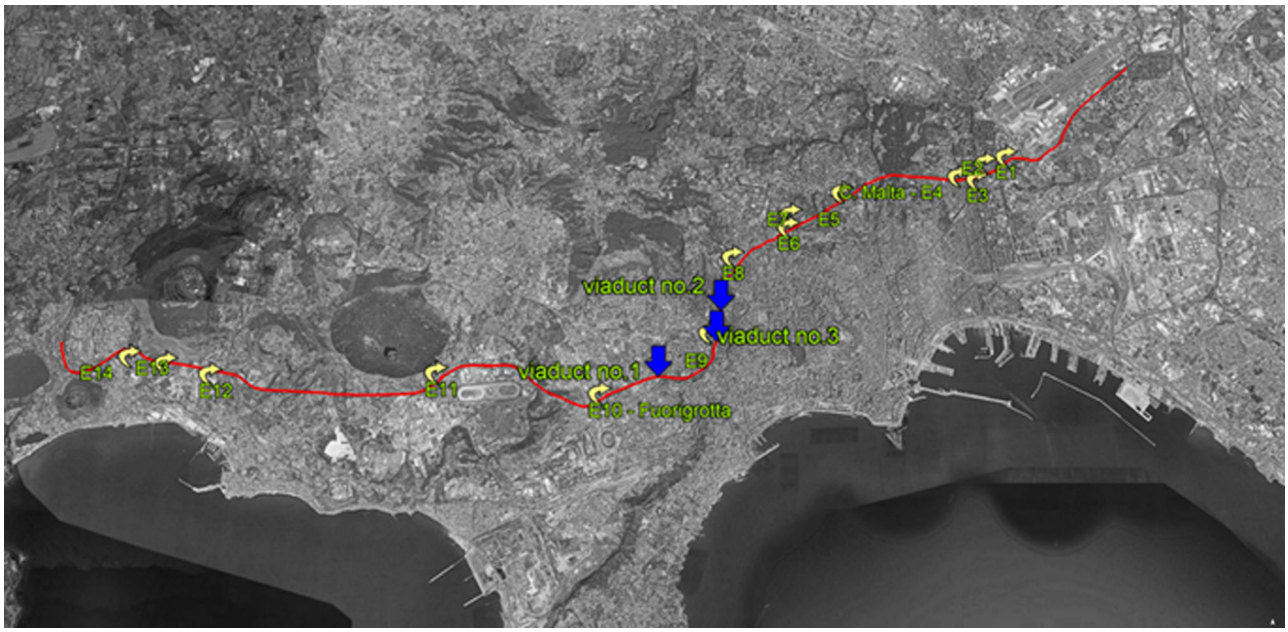

FIGURE 2 Layout of the A56—Tangenziale di Napoli—road network, with its 14 junctions and the three viaducts considered herein labeled

performed using conventional traffic loads recommended by building codes.

All the steps of the methodology described in this section, shown synoptically in the flowchart of Figure 1, are discussed in detail in the rest of the paper in the order they are performed.

3 | THE A56 (TAGENZIALE DI NAPOLI) HIGHWAY

A56—*Tangenziale di Napoli* is an urban highway connecting the various districts of Naples (Southern Italy), via 14 junctions, avoiding the relatively narrow downtown roads of the very densely populated city. At one end, it connects with the city's airport and with some major highway backbones toward the north and the rest of the south of Italy and at the other end with the suburban area of *Campi Flegrei* and *Litorale Domitio*; see Figure 2, where the junctions are indicated as E1-14. Its construction started in 1968, and in 1972, the first part opened to the public; however, only in 1992, it opened in its complete (current) configuration.

The highway length is about 22 km (from the Capodichino airport to the Campi Flegrei end, without considering the length of junctions) and the design capacity was 80,000 vehicles per day; however, the actual traffic in 2019 was about three times the design capacity. It is currently operated and maintained by Tangenziale di Napoli s.p.a., a company belonging to the national group of highway operators, Autostrade per l'Italia s.p.a.

The highway has uncontrolled access and toll booths at each exit junction. There are eight toll classes based on the number of axles per vehicle. A P2P speed control enforcement system is in place (Cascetta et al., 2011). The A56 highway has three lanes per direction. It has about 2 km of tunnels, and most importantly, it features multi-span bridges with a total length of more than 3 km (not including the viaducts of the junctions).

The viaducts are of various structural typologies with the dominant one being prestressed reinforced concrete simply supported spans. However, continuous beams and steel-concrete composite structures are also present. The network cannot accommodate special vehicles exceeding the size that can freely circulate on the Italian highway system because of the size of the toll booths.

4 | DEMAND ESTIMATION AND SUPPLY MODELING METHODOLOGY

Microscopic traffic simulation is used to propagate traffic demand over the highway network and to calculate the dynamic configuration of structural loads. The traffic simulations were aimed at estimating a probabilistic model of hourly OD demand flows over a 1 year reference period. They were not intended to calculate the unknown flows for the year at hand (i.e., 2018)—something that would require the application of predetermined methods for dynamic estimation of the daily OD flows (Antoniou et al., 2016). Once a yearly sample from such a distribution is

propagated through the network, simulated traffic shares the same statistical characterization of the measured traffic data (i.e., 2018 counts) from which the OD demand model has been estimated.

To simulate an entire year, 365 simulations have been run, each lasting 24 hr. This approach has been chosen because the state of the network, in terms of traffic, at the simulation initial instant, t_0, must be known to reproduce the traffic evolution for time $t > t_0$. Since the microscopic traffic initial state—which consists of position, speed, route, and destination of each vehicle in the network at t_0—is hardly ever observed or estimated, the only accurate solution to the initial state problem is to run a simulation lasting for the entire day. In this case, by starting the simulation at night, a condition of a quasi-empty initial network state can be assumed. Please note that a simulation period of an entire day is not common in traffic simulation practice, where shorter periods are usually simulated, and a preload traffic is applied to reproduce a gross proxy of the traffic on the network at the beginning of the simulation, that is, the initial state (Antoniou et al., 2016).

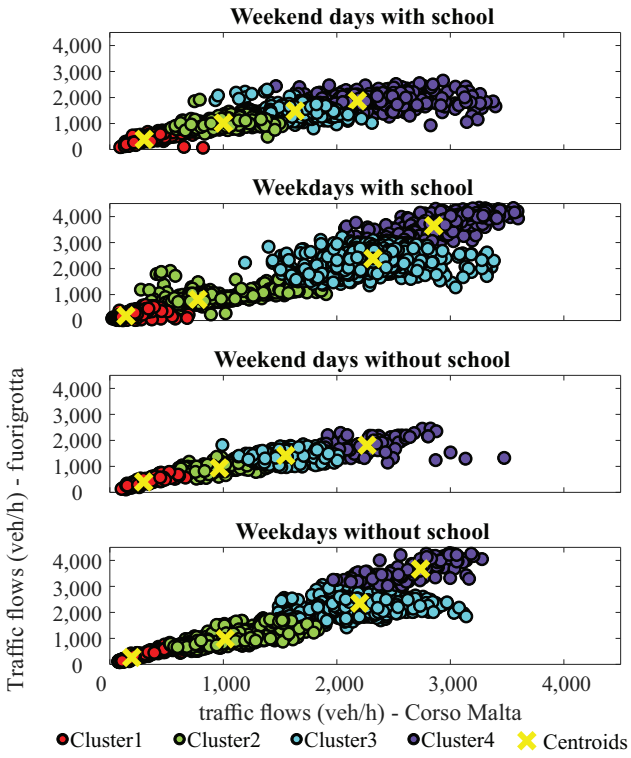

FIGURE 3 Clusters of hourly link flows

4.1 | Estimation of OD demand flows

As far as input demand is concerned, a 1-h interval has been considered suitable to reproduce traffic dynamics over the network with an adequate resolution for the scope of this analysis. Therefore, 365 daily series of 24 OD flow matrices have been estimated, for a total of 8760 hourly matrices. To this aim, hourly traffic counts—including those at all exit sections of the highway—were made available by the network's operator for an entire year (i.e., 2018).

The statistical characteristics at the basis of the estimation problem have been identified as (i) the *inter-day* (i.e., day-to-day) variability of link flows as measured by their coefficient of variation (CoV), and (ii) the *intra-day* (i.e., within-day) correlation of link flows as measured by the *Pearson correlation coefficient* (PCC) (e.g., Punzo et al., 2014). By applying measured CoV and PCC to a small number of base-case OD matrices, the hourly matrices of all days in a year have been estimated.

4.2 | Base-case OD matrices

A preliminary screening of link flows showed that yearly data could be divided into four groups, based on whether they were gathered during the school holiday summer months or during the remainder of the year and during workdays or non-workdays, such as weekends. Therefore, for each of these four periods, a cluster analysis has been run on all hourly link flows to identify hours with similar flow patterns.

In this framework, two representative locations across the network have been identified, namely, the *Corso Malta* and *Fuorigrotta* off-ramps (exit junctions). Then, a *k*-medoids algorithm (Arora et al., 2016; Jin & Han, 2011) has been applied on the hourly traffic flow pairs at the two locations, with varying cluster numbers. The algorithm's results for the case of four clusters are shown in Figure 3. In that figure, point markers corresponding to each identified cluster are shown in the same color (red, green, cyan, and purple for clusters 1 to 4, respectively) and each cluster's centroid is marked with a yellow cross. The number of clusters adopted (i.e., four) has been the best compromise found by the *k*-medoids algorithm to group the data. As expected, the clusters thus identified correspond to specific time slots in a day. In fact, with very few exceptions, all data gathered in the same period (i.e., the same hour of the day) from different days fell in the same cluster. However, the clusters do not correspond to the same hourly slots moving from one period to another one. As an example, the hourly slots that correspond to weekdays with school are shown. Referring to the colors in the figure, purple corresponds to the 6:00–10:00 a.m. slot, cyan to 10:00 a.m.–9:00 p.m., green to 9:00 p.m.–12:00 a.m., and red to 12:00–6:00 a.m.

Since the clusters found were not sparse, it has been assumed that for each time slot: (i) the OD flow's spatial structure is invariant within a time slot (i.e., given a period, all hours in a time slot share the same OD flow's spatial structure), and (ii) the common OD spatial structure is that estimated for the cluster centroid (i.e., using the traffic counts observed during the day and time corresponding to the centroid).

For each period and each cluster centroid (yellow crosses in Figure 3), an OD matrix has been estimated by means of a *generalized least squares* estimator (Cascetta et al., 2011), combining the information from observed link flows with a priori estimate of OD matrices available from previous planning studies of the network's operator. As a result, 16 base-case hourly OD matrices have been estimated (four clusters per period). In turn, these matrices have been used as the a priori information to estimate the 24 hourly matrices of the representative day of each period.

4.3 | Daily OD matrix estimation

For each period, the four estimated base-case hourly OD matrices have been used to define a *typical* day for that period. Such a typical day is characterized by a number of hourly OD matrices per time slot, each equal to the OD matrix of that time slot centroid from cluster analysis. As stated above, the daily series of OD matrices for the other days of a period have been estimated considering the CoVs of the total link flow over the network in each specific time/hour of the cluster and the PCC of the total link flows over the 24 hr of the period. These two statistics have been assumed as representative of the day-to-day variability of OD flows and of the within-day correlation of OD flows within a time slot.

Figure 4 shows the histograms of the total link flows within the period of weekdays with school (of 2018) for the time slots referring to four hours (from 6:00 to 10:00 a.m.).

As an example of the analysis results, the matrix of the PCCs of the 24 hourly total link flows within the period weekdays with school of 2018 is shown in Figure 5, where reddish colors indicate PCC close to unity, according to the color bar. The figure shows that there is a high correlation between the link flows in the time slots from 6:00 to 11:00 a.m., which increase toward the time slot from 7:00 to 10:00 a.m., as expected, being a direct consequence of highly congested patterns within the peak hours. In general, a correlation is high between the day-time hours and also between the night-time hours. On the contrary, day-time link flows are poorly correlated with night-time link flows since the two flows have completely different trip motivation patterns (i.e., the fact that we observe a high traffic flow during a day does not imply anything about the flow that we are going to observe during the following night).

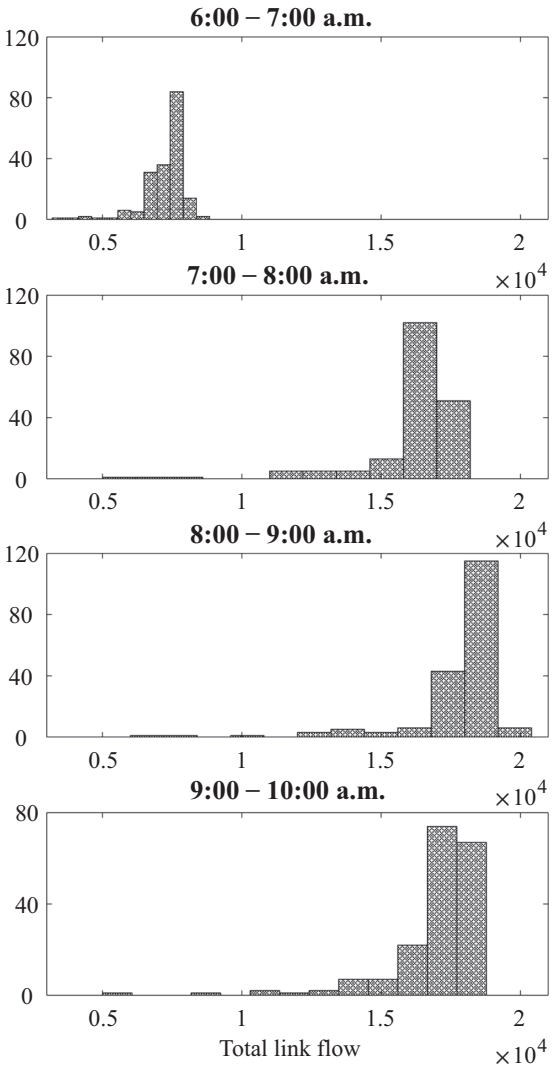

FIGURE 4 Histograms of the link flows of 4 hr within the period weekdays with school of 2018

Given a period, based on the typical daily matrices, on the CoVs of hourly total link flows, and on the correlations of the link flows within a day, a multivariate Gaussian copula has been defined (Rafati Fard & Shariat Mohaymany, 2019). On a side note, it should be pointed out that Gaussian is the only copula supported by the micro-simulation software at disposal, which somewhat limits the modeling choice.

The OD flow copula has been defined by the vector of 24 means and 24 standard deviations of the OD flow of each hour (where the means have been obtained from the OD correction procedure, and the standard deviations have been obtained by multiplying each mean by the corresponding CoV of the total flow exiting the network, in the same hour, computed from data), and by the 24 by

TABLE 1 Vehicle classes and geometry

Toll class	Type	ID	L	L_1	L_2	L_3	L_4	L_5
	–	–	m	m	m	m	m	m
II	Car < 4.5 m	car1	3.75	0.70	2.40	–	–	–
	Car ≥ 4.5 m	car2	4.60	0.90	2.80	–	–	–
	Truck	A2	8.40	1.30	6.00	–	–	–
	Bus	B2	10.70	2.40	5.40	–	–	–
	Van	VAN	4.85	0.90	3.10	–	–	–
III	Truck	A3	9.85	1.40	4.80	1.40	–	–
	Articulated lorry	AA3	12.50	1.40	3.70	5.90	–	–
	Trailer truck	AT3	18.75	1.40	5.60	7.90	–	–
	Bus	B3	15	2.80	9.50	1.30	–	–
IV	Truck	A4I	10.23	1.50	1.95	3.20	1.60	–
	Truck	A4II	13.26	1.45	4.10	1.35	1.35	–
	Articulated lorry	AA4	12.50	1.45	3.70	5.00	1.35	–
	Trailer truck	AT4	18.75	1.40	5.60	4.85	5.80	–
V	Articulated lorry	AA5I	16.50	1.45	3.40	1.30	5.90	1.30
	Articulated lorry	AA5II	16.50	1.40	3.70	4.70	1.30	1.30
	Trailer truck	AT5	18.75	1.40	4.80	1.35	5.00	5.45

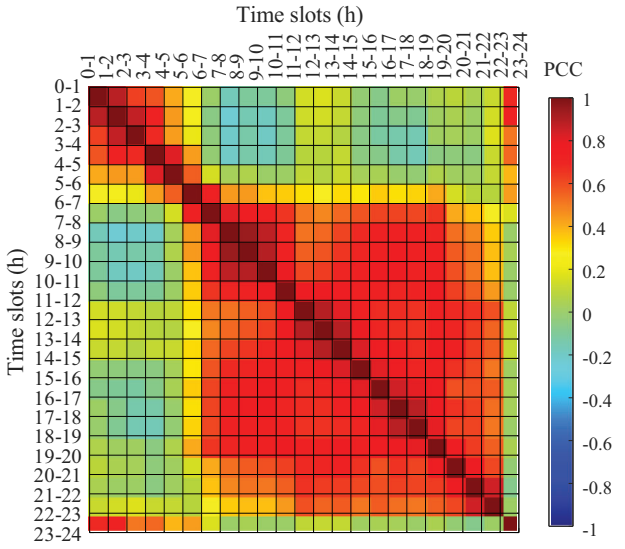

FIGURE 5 Matrix of the Pearson correlation coefficients of the 24 hourly total link flows for the period weekdays with school of 2018

24 correlation matrix of the total flow exiting the network computed from data, which have been assumed to represent also the time correlation of OD flows. Then, 24 hr series of OD flows have been generated from the copula for the number of days in that period via Cholesky decomposition. By repeating the same approach for each of the four periods considered, 365 series of 24 hourly OD matrices have been obtained, which are the sampled input for one-year traffic micro-simulations.

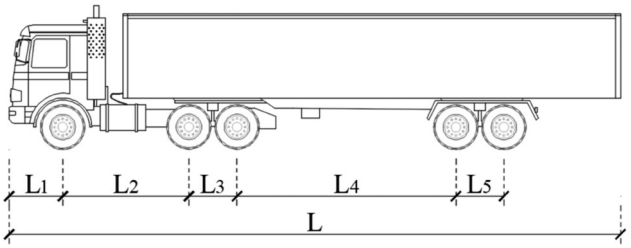

FIGURE 6 Geometry of articulated lorry subclass AA-5II

4.4 | Toll classes and vehicles

To completely define the traffic model, it has been necessary to characterize the vehicles circulating on the infrastructure. To account for vehicle heterogeneity, a multi-class traffic model has been developed, in which each vehicle class has its specific set of parameters.

On one hand, the network operator provided four macro-classes based on toll classes (denoted by numerals II, III, IV, and V), depending on the number of axles, from two to five. On the other hand, according to the Italian highway regulation (D.Lgs n.285/1992, 1992), 16 subclasses of vehicles have been defined to also consider the variability of vehicle geometry (i.e., axle position) within each toll class so as to properly assess the structural load from each vehicle as discussed in Section 6.1. Table 1 reports the toll classes and further subclasses considered.

Figure 6 shows an example vehicle subclass geometry, defined by the total length of the vehicle, L, and the

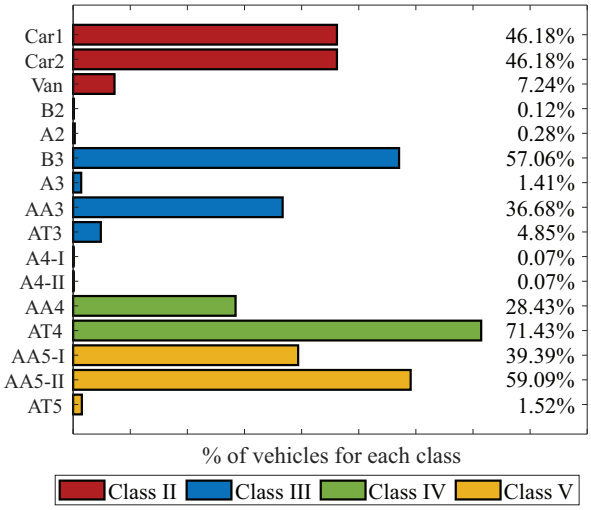

FIGURE 7 Percentile breakdown of vehicles per subclass

distances between the axles. The lengths and axle distances used for the definition of vehicle geometries for each subclass have been assessed based on data provided by vehicle manufacturers. More specifically, the average values from among available specifications (collected by the authors and available upon request) have been assigned to each subclass.

The road network operator provided the percentage of vehicle transits in 2018 per toll class (98.94%, 0.28%, 0.36%, and 0.26% from Class II to Class V). Therefore, a further subdivision into each of the 16 subclasses has been made by assuming that the distribution of vehicle types circulating on the network is the same as that of the vehicle fleet in the official regional database of registered vehicles (Automobile Club D'Italia, https://www.aci.it/). The percentage of each vehicle subclass within the toll classes is shown in Figure 7.

4.5 | Calibration of micro-simulation model parameters

The simulation model (implemented in Aimsun, https://www.aimsun.com/) required a calibration; that is, to minimize the differences between observed and simulated lane flows. The simulation-based calibration has been performed based on the methodology described in the literature (Ciuffo et al., 2008). The calibration procedure uses a *OptQuest/Multistart* heuristic (Ugray et al., 2005) to search for values of the continuous and discrete parameter sets, denoted by β and γ, respectively, that satisfy an optimization function:

$$\{\beta,\gamma\} = \text{argmin}\left\{RMSE\left[M^{obs}, M^{sim}(x_1, x_2, \ldots, x_h, \beta, \gamma)\right]\right\} \quad (1)$$

TABLE 2 Parameters for light and heavy vehicles

Veh.	a	b_n	b_m	RT	RT_1	RT_2
–	m/s^2	m/s^2	m/s^2	s	s	s
Light duty	3.00	4.00	6.00	0.40	0.80	0.80
Heavy duty	2.50	3.00	6.00	0.90	1.60	1.60

where *RMSE*, is the root mean square error between the observed and simulated sets of traffic measurements, M^{obs} and M^{sim}, respectively. Finally, $x_1, x_2, \ldots, x_h$ are the OD flows of the time interval h. Note that the parameters to be found are constrained to be within assigned bounds.

The optimization problem in Equation (1) has been applied sequentially to different parameters using different sets of measurements. First, the mean and standard deviation of service rates at the exit toll booths have been calibrated. Peak-hour exit flows at the Corso Malta toll booths have been considered since vehicle queues feed those booths continuously at peak hours (i.e., a period when booths operate at full capacity, and therefore the resulting exit times are only dependent on toll booth service rates). In fact, accurate calibration of toll booth capacity is crucial to realistically reproduce the queue spillback from the off-ramp into the highway, which occurs at the Corso Malta exit junction daily.

A calibration of the off-ramp model parameters has been then carried out to qualitatively reproduce the site-specific behavior of vehicles at that critical off-ramp junction. Desired speeds, maximum acceleration and deceleration rates, reaction times, and speed acceptance (which is a parameter representing the level of compliance with the speed limit of a vehicle) for the light-duty (LD) vehicle classes (i.e., car and van) and heavy-duty (HD) vehicle classes (i.e., bus, truck, and lorry) have been then calibrated, by solving the problem in Equation (1) against highway lane flows—available from the highway P2P speed enforcement system; see Cascetta et al. (2011) for a description of data available from the P2P system. For a discussion of Gipps' model, which is the car-following model applied in Aimsun, its parameters and corresponding bounds, see Ciuffo et al. (2012) and Punzo et al. (2012). Note that all HD vehicle classes share the same values of parameters. Eventually, a further refinement of toll booth service rate parameters has been performed to account for the change in calibrated toll booth flows (at capacity) due to the calibration of car-following model parameters. Table 2 lists the acceleration of the vehicle, a, and the normal, b_n, and maximum, b_m, deceleration, that is, the deceleration in normal traffic condition and dangerous situation (e.g., late-recognized traffic jam), respectively. Moreover, the calibrated parameters for reaction time (for a stimulus, RT, at stop, RT_1, or at barrier, RT_2) are listed. Furthermore, the calibrated value for the speed acceptance

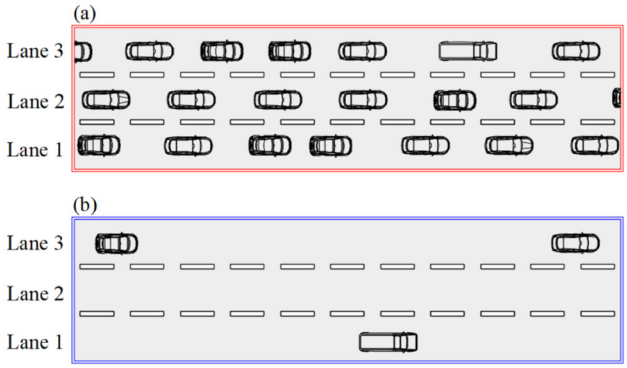

FIGURE 8 Snapshots of congested (a) and free-flow (b) traffic condition

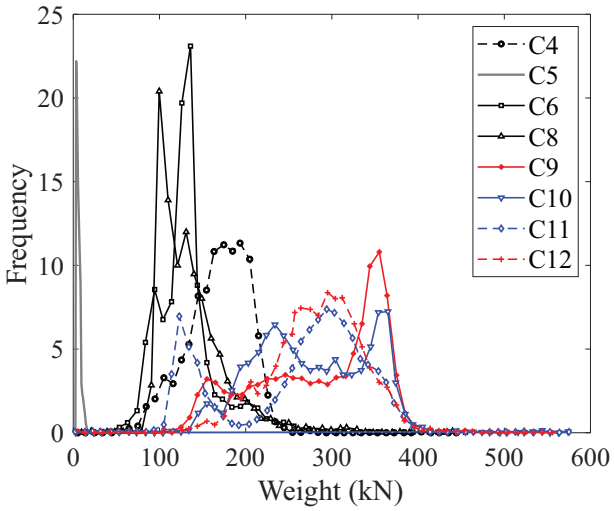

FIGURE 9 Distributions of total weight

parameter for HD vehicles resulted equal to 0.83 (with the exception of a 0.85 value obtained for A2 trucks) and for LD vehicles equal to 0.91 (except for buses for which the value resulted 0.86).

Note that the traffic flow algorithm handles the situation where trucks are in adjacent lanes, which is significant for extreme loads on multi-lane bridges.

4.6 | Traffic simulation

The traffic simulation provides information such as vehicle flow, density, and average speeds, depending on the position of virtual recorders placed along the network. Although the default output of the software is not necessarily exhaustive for research purposes, further information can be extracted by means of an application programming interface. In fact, the simulation output data required for this study include vehicle trajectories, consisting of position and speed for each vehicle (characterized by a unique ID, class, length, and width), that are recorded at a sampling rate of 10 Hz.

As an example of simulation results, Figure 8 shows two snapshots of traffic on a road segment, one corresponding to *congested* traffic conditions and another showing a *free-flow* traffic situation.

Apart from vehicle trajectories (referring to the front bumper of the vehicle), two more pieces of information are necessary to derive the load configurations on bridges; that is, the geometry and weight of each vehicle. Each vehicle's axle positions are derived from this information according to its pre-assigned geometry from Table 1.

5 | BRIDGE ANALYSIS

Three case-study bridges of the A56 are considered herein. In this section, these structures are described along with the operations needed to derive the load configurations, that is: (i) the attribution of total weight to each vehicle, (ii) its distribution among the axles, and (iii) the definition of load configurations for the bridges from the results of the micro-simulations. Additionally, the code-based load configurations are described f with the simulation results.

5.1 | Vehicle weight and axle load

For the car and van vehicle subclasses, deterministic weight values have been attributed from manufacturer specifications (ANFIA, https://www.anfia.it/it/), while for the bus, trucks, and lorries subclasses, weight attribution has been based on empirical distributions (Lu et al., 2002). More specifically, the considered study provides truck traffic data collected from 1991 to early 2001 by the California state highway network WIM system in the United States. The report was aimed at representing the axle load frequency distributions for the various axle groups within all truck types that pass on the road network. Although that study provides a breakdown of the data with respect to the data-gathering period (i.e., day/night), seasonal weather conditions, and geographical position of the monitored sections within the road network, herein only the marginal load frequency distributions per year provided for each truck type are considered. In this context, Figure 9 shows the empirical weight distributions considered. In the figure, these distributions are plotted for eight vehicle categories, labeled using the nomenclature of the original study. These categories correspond to very light vehicles (C5 in grey), vehicles whose weight ranges between 100 and 200 kN (C4, C6, and C8 in black), vehicles whose

TABLE 3 Weight distribution per axle

Vehicle ID	No. of axles	Axle type(s)	Associated distribution (Figure 9)	Load % per axle
A2	2	S+S	C5	51; 49
B2	2	S+S	C4	46; 54
A3	3	S+T2	C6	37; 63
B3	3	S+T2	C4	47; 53
AA3	3	S+S+S	C8	38; 18; 44
AT3	3	S+S+S	C11	20; 36; 44
$A4_{(I)}$	4	S+S+S+S	C8	26; 24; 13; 37
$A4_{(II)}$	4	S+T3	C8	24; 38; 38
AA4	4	S+S+T2	C8	36; 13; 51
AT4	4	S+S+S+S	C11	21; 29; 31; 19
$AA5_{(I)}$	5	S+T2+T2	C9	22; 22; 56
$AA5_{(II)}$	5	S+S+T3	C10	25; 5; 35; 35
AT5	5	S+T2+S+S	C12	19; 33; 16; 32

Note: A = truck; B = bus; AA = articulated lorry; AT = trailer truck; S = single axle; T2 = tandem; T3 = tridem.

weight ranges between 200 and 400 kN (C10 and C11 in blue), and vehicles within the same range characterized by bimodal weight distributions (C9 and C12 in red).

Each vehicle subclass considered, except for the three characterized as cars or vans, has been assigned one of these empirical annual weight distributions as shown in Table 3. Thus, each vehicle of the micro-simulation has been assigned a total weight value by sampling the associated distribution.

Once the weight of each vehicle is obtained, its distribution among the axles (which are of three types, S for single wheels, T2 for tandem wheels, or T3 for tridem wheels) has been determined from the support reactions of simple static schemes representing the frames of the considered vehicles (Grakovski et al., 2020).

For example, Figure 10a shows the simply supported beam used to represent the frames of cars, bus, and truck subclasses (labels A2, A3, B2, B3, AT4, AT5 in Table 3); Figure 10b shows the static scheme associated with the articulated trucks (AA and AT3), which is a scheme obtained as the composition of two simply supported beams; and Figure 10c shows the static scheme associated with trailer trucks ($A4_{(I)}$ and $A4_{(II)}$), which is a continuous beam. In this context, it has been assumed that the vehicles are loaded in a uniform manner (this is considered acceptable because in practice there is a tendency to load vehicles as evenly as possible) and that vehicle self-weight has been included in that uniformly distributed load for simplicity. Therefore, each beam support reaction, expressed as a fraction of the total load, represents the weight percentage that each axle applies on the road or bridge deck as a static load.

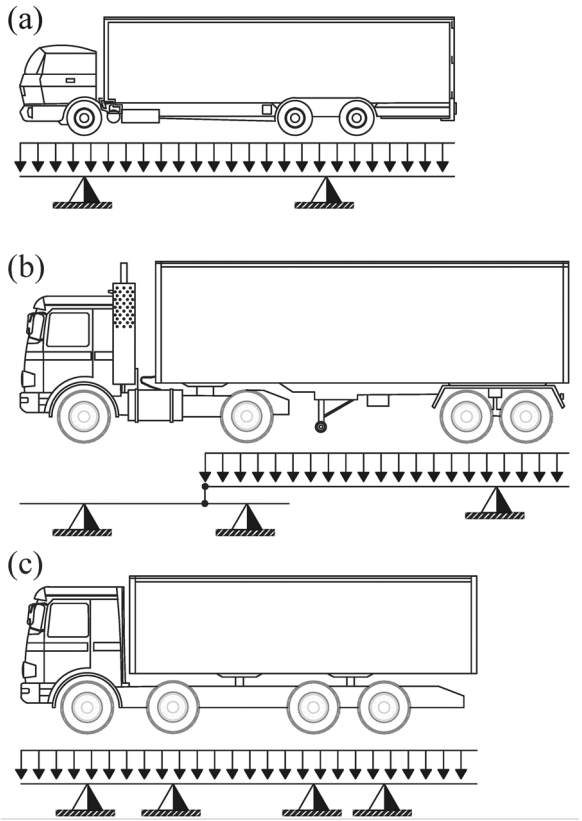

FIGURE 10 Schemes for the distribution of the total weight among the axles

Table 3 summarizes the results obtained for each type of vehicle, where the last column reports the load percentage per axle. Finally, note that the tandem axle, T2, has been represented by a single support reaction because the distance between the axles is lower than the selected discretization length along the road (to follow). For similar considerations, the tridem axles are represented by two equal reactions.

Note that the applicability of the US data discussed in this section in the context of the A56 highway should be verified by comparison with suitable WIM information from Italy. To date, these studies are yet not available. Thus, such applicability should be taken as a working assumption.

5.2 | Case-study bridges

For the purposes of this study, three viaducts along the network have been selected as benchmarks for calculating the effects of the simulated traffic loads in terms of structural demand, namely, the *Miano-Agnano* (No. 1), *Arena Sant'Antonio* (No. 2), and *Calata San Domenico* (No. 3) viaducts, whose position along the road network is shown in the map of Figure 1. The three viaducts feature twin

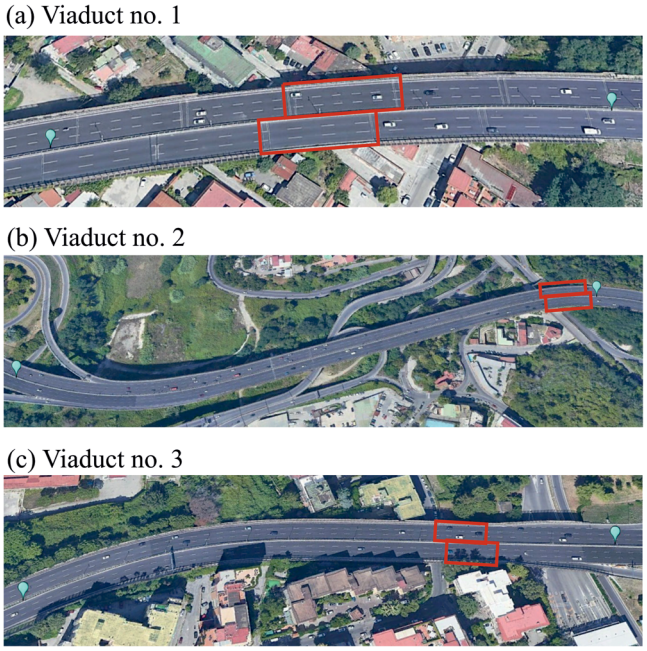

FIGURE 11 Case-study viaducts top view: (a) Miano Agnano—No. 1, (b) Arena Sant'Antonio—No. 2, and (c) Calata San Domenico—No. 3

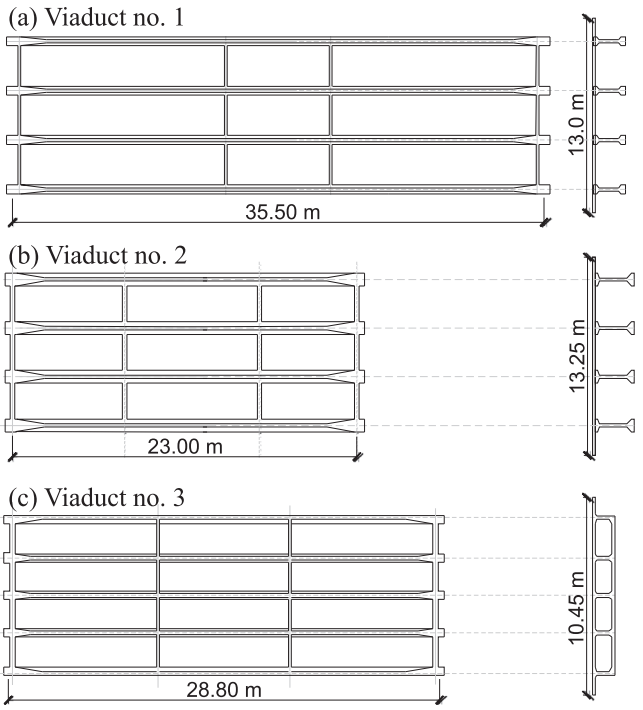

FIGURE 12 Plan- and cross-section of a typical span of the viaducts (a) No. 1, (b) No. 2 and, (c) No. 3

superstructures, one per traffic direction, mostly consisting of consecutive simply supported spans and single- or double-column reinforced concrete piers with cap beams.

The superstructure of the Miano-Agnano and Arena Sant'Antonio viaducts is composed of precast prestressed concrete girders, post-tensioned with a span length between supports of 35.5 m for the former and pretensioned with a typical span of 40.0 m (23.0 m for the end spans) for the latter, joined together via cast-in-place reinforced concrete deck slabs and transverse beams—a structural system that has seen widespread use in Italy since the 1960s (Menn, 1990). In both cases, a typical span comprises four precast girders, exhibiting a span-to-depth (slenderness) ratio of around 14.

For the girders of viaduct No. 1, part of the post-tensioning was applied after composite action with the deck slab had been established, while for the No. 2 girders, deviation points were provided for a part of the pretensioning strands, at one-third of the span, to provide a load-balancing effect.

On the other hand, the No. 3 viaduct features a mix of post-tensioned simply supported precast girders with a 28.8 m typical span and a Gerber system comprising post-tensioned multi-cell box girders.

For the sake of brevity, and also because it is not expected that the results would differ otherwise, a limited number of spans of each bridge has been considered, which are highlighted as red boxes in Figure 11 and also indicated in Figure 2.

5.3 | Structural modeling

For each case-study viaduct, the structural behavior of one representative segment has been modeled using assemblages of two-node beam-flexure finite elements (FEs). The underlying assumption of these models is that constituent materials of structural members remain within the range of linear elasticity under the loading conditions considered herein and that inertial effects of load application can be neglected. Material properties for each viaduct have been obtained from a series of in situ and laboratory tests commissioned by the network operator.

As mentioned above, a single typical span has been modeled for each viaduct; since the superstructures feature twin independent decks per the direction of traffic, a total of three structural models are needed. In the case of viaducts No. 1 and No. 2, due to the open girder-slab cross-section potentially experiencing deformation due to transverse bending, as can be seen in Figure 12, the superstructure has been modeled using a plane beam grid, and the model also accounted for the flexural stiffness of the cap beams, as the effect of the latter on the distribution of flexure among the girders can be non-negligible. In cases such as this, where the primary longitudinal girders are prestressed and the transverse partition is guaranteed via simply reinforced beam elements and deck slabs, the literature generally holds plane grid models as a good compromise between relatively simple numerical

modeling and realistic representation of the transverse stiffness since the latter may be affected by some limited cracking in-service conditions.

In the case of viaduct No. 3, the in-plane deformability of the multi-box girder's cross-section has been also modeled using a grid of longitudinal and transverse beam elements, with each of the former being attributed the flexural and torsional stiffness of a single cell and each of the latter representing the transverse flexural stiffness of the upper and lower slabs.

5.4 | Code-based safety analysis

Most structural safety analyses according to modern codes (AASHTO, 2020; ASCE/SEI 7–22, 2022; C.S.LL.PP., 2018; EN 1991-2, 2003) are performed at the cross-section level. They entail a comparison of factored sectional force demands, induced by external actions, such as permanent and traffic loads, with the corresponding load-bearing capacity calculated from the mechanical properties of the constituent materials. This is often formally expressed under the guise of a demand-against-capacity inequality:

$$E_d = \gamma_{G1} \cdot G_1 + \gamma_{G2} \cdot G_2 + \gamma_Q \cdot Q_k \leq R_d \qquad (2)$$

where G_1 and G_2 represent the sectional forces (e.g., bending moments, M, or shear forces, V) caused by the effect of structural and non-structural permanent loads, respectively, Q_k is the sectional forces due to traffic loads, and γ_{G1}, γ_{G2}, γ_Q are the so-called *partial-safety-factors* corresponding to each type of action.

For the types of bridge decks examined here, other actions due to prestressing or other environmental effects have been neglected from this inequality. Thus, the sum of factored external actions is the design structural demand E_d, and R_d is the nominal design resistance of the cross-section. In this context, operating safety margins for the structure can be conventionally quantified as the distance between factored capacity R_d and demand E_d.

The implication of this expression is that, as long as the demand on the left-hand side remains lower than the nominal capacity appearing on the right-hand side, the code's structural safety requirement can be considered satisfied.

The sectional forces due to all actions, traffic loads included, have been calculated using numerical models of the bridge structure, such as the ones presented previously. Traffic loads for calculating Q_k have been represented by conventional code-mandated load schemes consisting of a combination of point and distributed forces, such as those depicted in Figure 13, that can be considered to travel on the superstructure along the bridge axis. On the other hand, permanent loads G_1 and G_2 have been calculated based on nominal code-mandated material apparent densities, in combination with the design geometry of the structure and finishings.

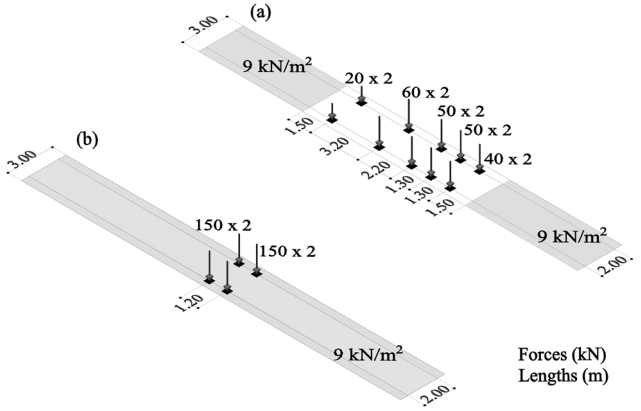

FIGURE 13 Isometric representation of a single-lane traffic load according to EN1991-2 Load Model 1 (a) and DM2020 load for bridges transitable by heavy traffic (b)

For the example of bridge load models for the design of new structures for the Eurocode (EN 1991-2, 2003) and Italian code (C.S.LL.PP., 2018), hereafter referred to as NTC18, shown in Figure 13a, the underlying assumption behind this conventional traffic load is that the sectional force demand Q_k, derived from its application to any bridge structure will represent a so-called *characteristic* value, that is, a value that is only exceeded every 1000 years on average (EN 1990, 2002).

It is also worth mentioning that codes imply that the characteristic value of any sectional force demand will be calculated by arranging the conventional traffic load model in the most unfavorable disposition for that specific action.

Recently, the emerging requirement for safety verifications of aging road infrastructure in Europe and elsewhere has highlighted the need to contemplate existing bridges, which may not satisfy the normative reliability prescriptions for new structures yet should remain open to traffic. In this direction, the Italian government has adopted guidelines DM2020 that introduce alternative partial safety factors and traffic load models to be used in decision-making to determine if a bridge can remain *operational* (open to traffic until the bridge is retrofitted) or *transitable* (open to traffic under limitations). Thus, to facilitate the adoption of traffic limitations in terms of maximum allowable vehicle weight, these load models are contemplated as convoys of vehicles whose dimensions and axle loads correspond to specific weight limitation thresholds.

For example, Figure 13b shows the load model to be used for determining if a bridge can remain transitable

TABLE 4 Partial safety factors for DM2020 and NTC2018

	DM2020	NTC2018
γ_{G1}	1.26	1.35
γ_{G2}	1.26	1.5
γ_Q	1.6[a]	1.35

[a]When the traffic restriction control system does not check all vehicles.

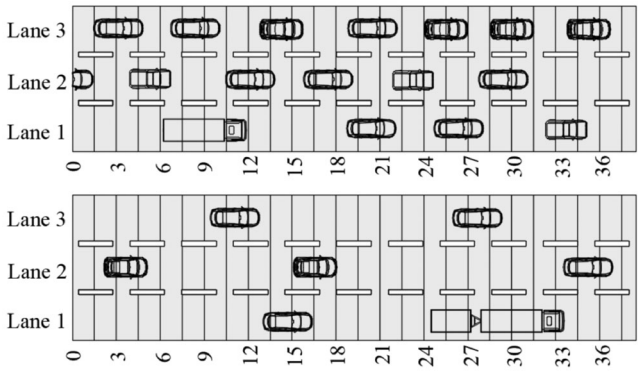

FIGURE 14 Example of two traffic configurations on a bridge deck from simulations

by heavy traffic; the vehicle weight threshold to impose in this case is 440 kN (equal to the sum of point loads shown). In contrast to the Eurocodes, DM2020 does not associate a specific exceedance return period to the actions produced on bridges by this alternative load model. Not only this but also the partial safety factors prescribed for the Equation (1) safety check differ between the two cases of up-to-code and transitable bridges. These factors are listed in Table 4.

5.5 | Traffic-induced bridge loads

Traffic micro-simulations return the position of each vehicle at each time step. To obtain the vehicle positions along the bridge deck, the latter has been discretized in cells of 1.5 x 3.0 m, and each cell can be loaded by a single vehicle axle at a time. Figure 14 shows, as an example, two vehicle configurations recorded on viaduct No. 1 at a certain time instant of a school weekday from the simulation, while Figure 15 shows the two axle-force configurations corresponding to the traffic snapshots in Figure 14.

From these traffic load configurations, the corresponding internal forces to which the bridge is subjected can be calculated using the FE models described above, at least under the simplifying assumption that only a static gravity load effect is considered, neglecting inertial effects due to vehicle acceleration/deceleration.

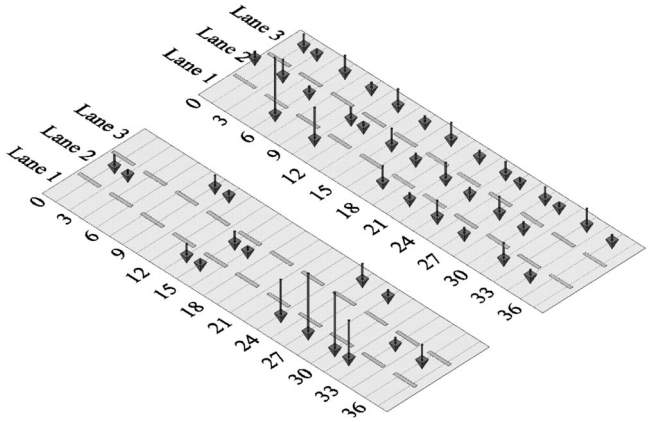

FIGURE 15 Spatial distribution of forces corresponding to the vehicles of Figure 14

6 | RESULTS AND DISCUSSION

Based on the post-processing of the results of the simulations discussed above, it has been possible to assess the distribution of the structural demand induced by vehicular traffic in each of the considered bridges and to compare it with the demand estimated by means of the traffic models defined by the codes. To this aim, reference cross-sections have been considered for each structure (i.e., sections at midspan or near the supports of the girders for bending moment and shear actions) where the internal forces are to be calculated. For these cross-sections, the traffic-induced structural actions have been evaluated at each time step (0.1 s) of every simulated day. The resulting daily distributions of sectional forces have then been used to build probabilistic models for the daily and annual maxima of the actions, Q, that each viaduct experiences due to simulated vehicular traffic, for each of the 4-day clusters identified. Subsequently, these probability models have been used to compute quantile values of the traffic-induced actions from simulation corresponding to the code's assumption for the characteristic value, Q_k, that appears in the safety verification of Equation (2), which in turn has enabled the comparison between the application of bridge-specific and code-based models.

6.1 | Probabilistic modeling of traffic-induced structural actions

In the representative spans of the case-study viaducts examined here, the critical sectional forces that govern the overall load-bearing capacity are considered to be flexural moments at midspan of the longitudinal prestressed concrete girders and shear forces of the same girders near their supports. According to the procedure described in the

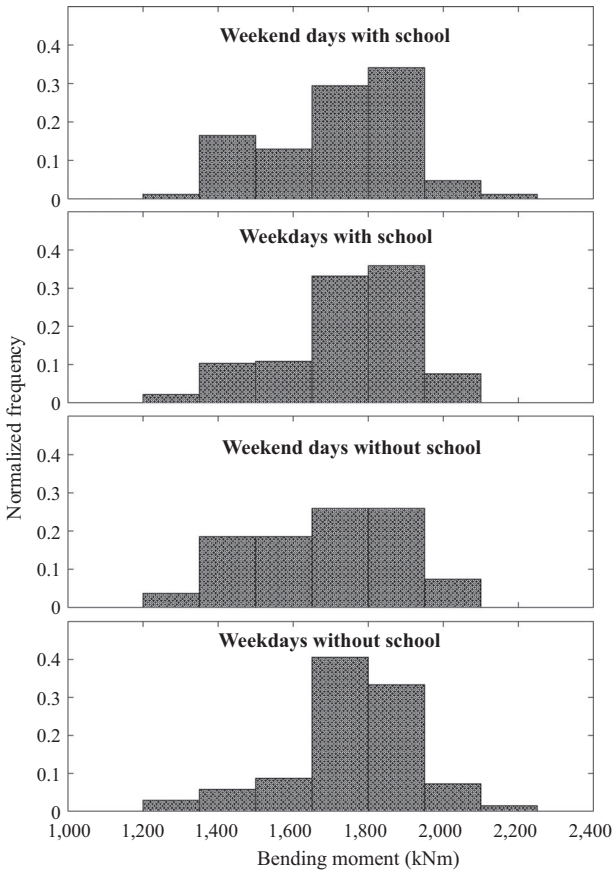

FIGURE 16 Daily maximum values for bending moment at midspan of viaduct No. 1

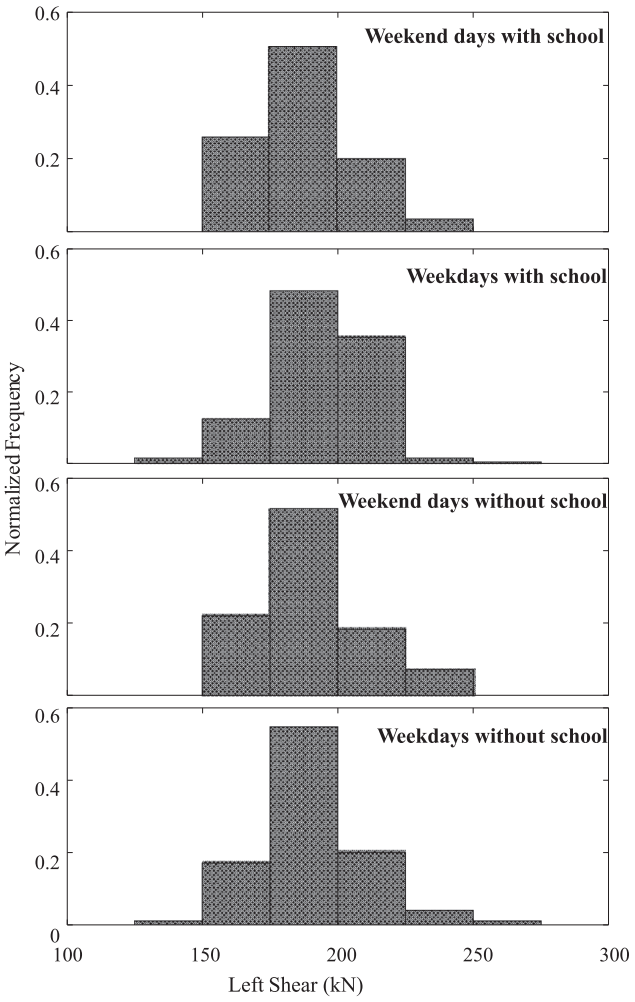

FIGURE 17 Daily maximum values for shear at the left support of viaduct No. 1

previous sections, for each time step of simulated traffic, the corresponding disposition of loads on the superstructure can be assigned, and the FE models can be used to provide flexural moments and shear forces at these reference cross-sections, that is, the traffic-induced structural actions. From these results, it is possible to determine the largest (absolute) value of each action appearing on each viaduct span and reference cross-section for every simulated day of traffic. As an example, these simulated daily maximum values can be seen in Figures 16 and 17, in the form of a normalized frequency histogram for each typical day, with the former corresponding to the daily maximum bending moment at midspan of the No. 1 viaduct and the latter to shear at the left support. In other words, for each of the 365 simulated days of traffic, only the daily maximum value is preserved from each sectional force's simulated time series for further processing, and these figures can be considered to represent the shape of the empirical distribution of these daily maxima.

It has been then assumed that, for each of the four typical days established via cluster analysis, these simulated daily maxima of traffic-induced actions were realizations of four random variables Q_j, $j = 1,..,4$, that all follow Type II extreme value (EV) distributions. This seemed a rational choice given the conditions under which the EV distribution is the asymptotic model for maxima (Benjamin & Cornell, 1970. Thus, the cumulative distribution for the jth typical day was given by:

$$P\left[Q_j \leq q\right] = e^{-\left(\frac{u_j}{q}\right)^{k_j}} \tag{3}$$

where u_j and k_j are parameters that, in this case, have been estimated for that day by matching the first and second moment of the distribution to those of the simulated daily maxima. These parameters for M at midspan and V at the left support of viaduct No. 1, for all four typical days, are given in Table 5.

Once an EV model was fitted against the data of each typical day, the probability distribution of the annual maximum traffic-induced action on each viaduct's primary girders, Q^*, has been then evaluated assuming independence among the four typical days clusters and among

TABLE 5 Extreme value Type II distribution parameters for M at midspan and V at the left support of viaduct No. 1

	M		V	
	k_j	u_j	k_j	u_j
Weekend days with school	12.49	1639.1	13.81	181.16
Weekdays with school	13.96	1672.3	14.02	185.16
Weekend days without school	11.82	1604.2	14.13	179.60
Weekdays without school	14.62	1679.4	13.43	182.04

traffic demands in each day of the clusters:

$$P\ [Q^* \le q] = \prod_{j=1}^{4} P\left[Q_j \le q\right]^{n_j} \tag{4}$$

where n_j is the number of days in a year for the jth typical day, and $P[Q_j \le q]$ is the cumulative distribution for that day, obtained by the fitting procedure described above.

This result can then be used to calculate the one-tenth upper quantile of the annual maximum distribution, $q_{0.1\%}$, that is, the sectional force value for which $P\ [Q^* > q_{0.1\%}] = 0.001$. This value represents actions having a 1000-year return period, same as the code-mandated characteristic value Q_k.

6.2 | Bridge-specific versus code-based safety margins

The values $q_{0.1\%}$, calculated from the probability distribution of the annual maximum traffic-induced actions, can be compared to the characteristic values derived from the code-based load models to investigate the safety margins between the application of bridge-specific and code-based models. Indeed, for each bridge characterized by a predetermined structural capacity, the comparison between traffic-induced and code-based demand shows the effect of considering bridge-specific traffic conditions in structural safety checks. It should be noted that the traffic simulations carried out for this study do not take traffic limitations into account, consistent with the requirements of the load models proposed in the Eurocode. On the other hand, the load model proposed in DM2020, for existing bridges that can remain transitable by heavy loads, considers a traffic limitation (i.e., vehicle weight threshold). Therefore, the comparison between the actions is more consistent in the former case than in the latter.

6.3 | Actions induced by traffic

The traffic-induced actions alone are compared first; that is, structural and non-structural permanent loads are not considered. To this aim, Figure 18a shows the distribution of the annual maximum of the bending moment at midspan for the No. 1 viaduct due to the traffic load from Equation (4). The vertical lines on the figure represent some notable values. More specifically, the $q_{0.1\%}$ value is indicated by a blue line. It is recalled that $q_{0.1\%}$ corresponds to a return period of 1000 years, that is, the code-prescribed (EN 1991-2, 2003) return period for Q_k in Equation (2). The distances between the values marked with the blue lines and the corresponding highest values appearing in the histograms of Figures 16 and 17 provide an indication of the inherent very large extrapolation in obtaining the $q_{0.1\%}$ value from a probability model. For example, the $q_{0.1\%}$ value moment and shear force for viaduct No. 1, are approximately twice the highest daily maximum obtained from the 1-year simulation. Finally, the green and black lines specify the M values calculated by considering the load models of DM2020 for bridges transitable by heavy traffic and of EN1991-2, respectively, which are the load configurations shown in Figure 13.

For viaducts No. 1 and No. 3, Figure 18 shows that the bending moment, calculated with the traffic simulation data specific to the bridge, is lower than both the code-compliant ones, the former being roughly between two-thirds and one-half of the latter. On the contrary, for viaduct No. 2, the M values calculated with traffic simulation data and the load model of DM2020 deviate by only 10%. Although the code-compliant load configurations are not dependent on the bridge-specific traffic, they can provide forces that are in variable ratios with each other due to the viaduct geometry. The legend of Figure 18 also lists the return period of the actions calculated with the code-compliant load model.

Figure 19 provides the same type of information as Figure 18, only for shear, V, at the viaducts' deck supports. For the No. 1 and No. 3 viaducts, the ratio of simulated-to-code-mandated actions for V is quite similar to those for M, while for the No. 2 viaduct, the shear calculated according to DM2020 is lower than the one calculated with the simulation, and its estimated return period is only 69 years. This can indicate that the control of the traffic limitation (i.e., weight threshold equal to 440 kN) must be very strict for the safety of this viaduct because the probability that, in the absence of control, the limit is exceeded on this viaduct is greater than for the other two viaducts.

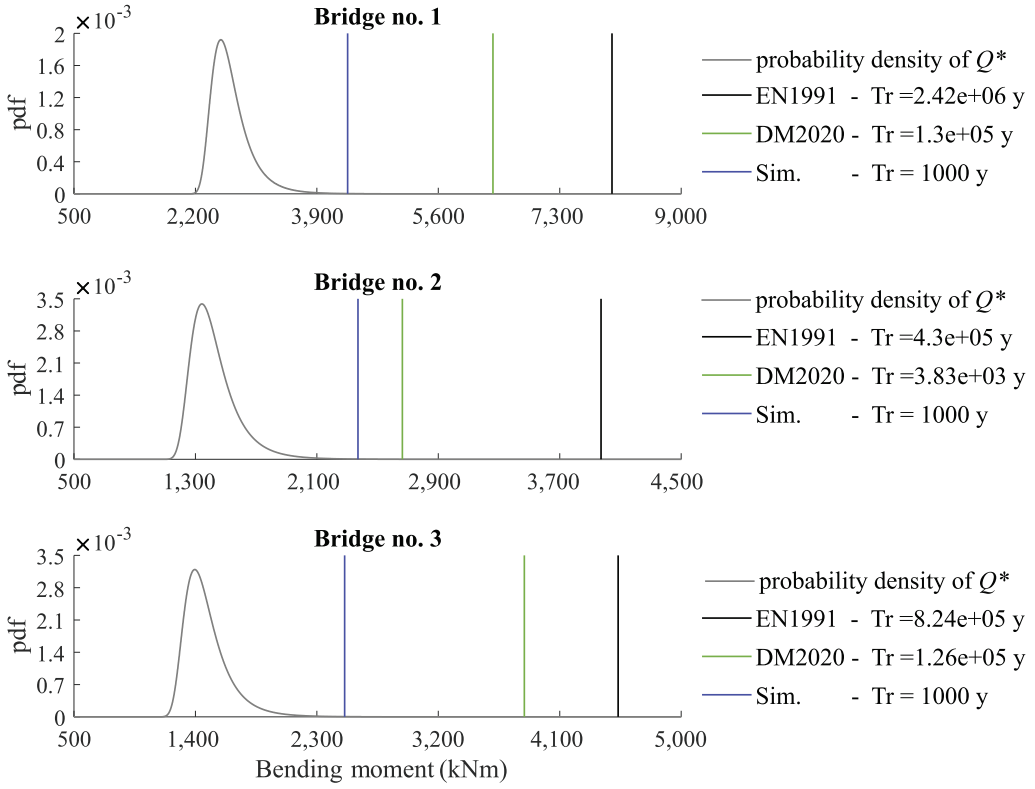

FIGURE 18 Maximum bending moment at midspan due to moving load: (a) viaduct No. 1, (b) viaduct No. 2, and (c) viaduct No. 3

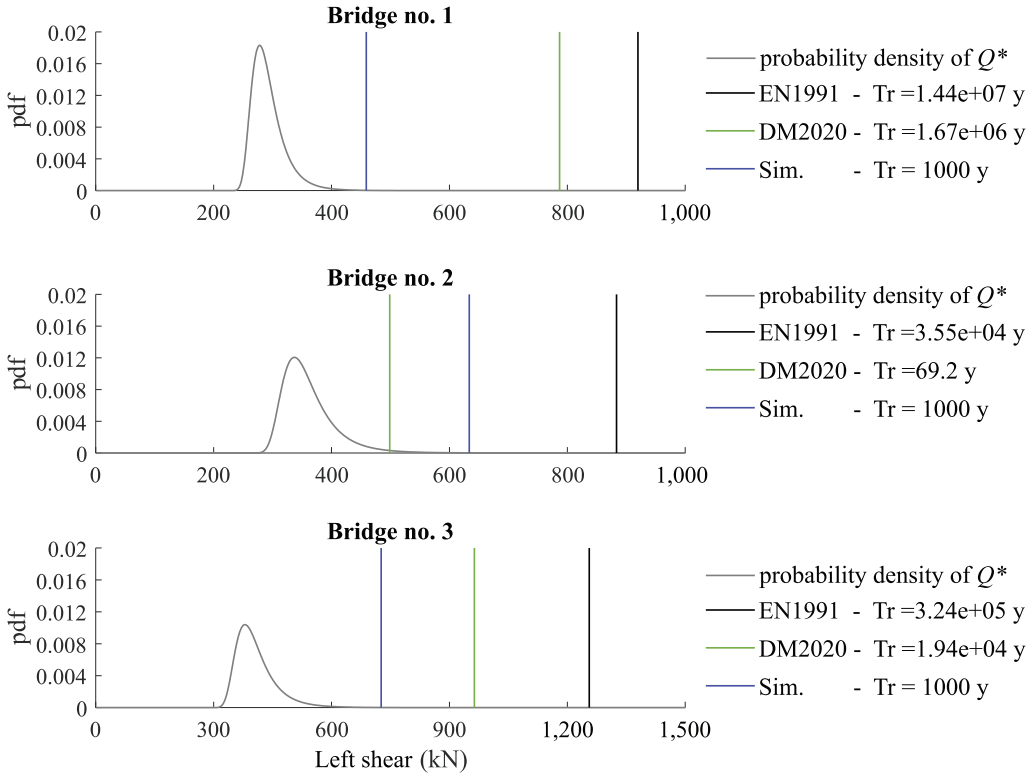

FIGURE 19 Maximum shear at the left support due to moving load: (a) viaduct No. 1, (b) viaduct No. 2, and (c) viaduct No. 3

TABLE 6 Ratio between bridge-specific and code-based characteristic quantiles of bending moment, M, and shear, V, due to traffic load

	EN1991-2 load model		DM2020 transitable to heavy traffic load model	
Viaduct	***M***	***V***	***M***	***V***
No. 1	0.54	0.50	0.68	0.58
No. 2	0.60	0.72	0.89	1.27
No. 3	0.55	0.58	0.65	0.75

TABLE 7 Ratio between factored values of bending moment, M, and shear, V, due to traffic and permanent loads

	EN1991-2 load model		DM2020 transitable to heavy traffic load model	
Viaduct	***M***	***V***	***M***	***V***
No. 1	0.77	0.75	0.84	0.78
No. 2	0.79	0.84	0.95	1.13
No. 3	0.80	0.74	0.84	0.85

For the sake of clarity, Table 6 summarizes the ratios of the $q_{0.1\%}$ values from the simulations and the code-specified Q_k. For the EN1991-2 load model, the values of these ratios range between 0.50 and 0.72 indicating that the bridge- and network-specific action quantiles are generally lower than their code-mandated counterparts. For the DM2020 load model, they range between 0.58 and 1.27. In this case, a ratio below unity indicates that the conventional traffic limitation load model corresponds to action values that would otherwise be exceeded on average less frequently than once every thousand years. However, the larger-than-unity ratio encountered in one case indicates that the limitation condition corresponds to actions that are apparently exceeded more often than that. Therefore, this highlight the importance of a control system for traffic limitation measures.

6.4 | Combined actions

As previously discussed, actions due to permanent loads and variable actions due to traffic loads must be combined according to Equation (2). Therefore, safety margins should be calculated based on the factored values of M and V due to the combination of traffic, permanent, and possibly other, loads. In this context, Table 7 shows the ratios between the design actions E_d obtained by considering the bridge-specific traffic load characteristic values from simulation in Equation (2) to those from the code-mandated values, both calculated using the partial safety factors from Table 4. These ratios have been calculated for both moments and shear forces of all three bridges. The resulting values range between 0.77 and 0.84 for the EN1991-2 load model and 0.78 and 1.13 for the DM2020 transitable to heavy traffic load model. These ratios of structural demands can be regarded as relative measures of each viaducts' safety margin between the two definitions of traffic-induced actions. From the values in both tables, it is apparent that these safety margins can vary even between bridges with similar structural configurations, belonging to the same network.

7 | CONCLUSION

In the current approach to the code-based safety assessment of bridges, traffic loads are defined based on the exceedance return period of the structural actions they determine. This could require detailed traffic monitoring, which is seldom feasible at the infrastructure scale. In the study, it was explored whether traffic micro-simulations, in conjunction with structural modeling, can surrogate/complement monitoring.

The study considers the real case of the urban highway of Naples (Italy), hosting about 240,000 transits per day and featuring several major viaducts.

The calibration of the input to traffic simulations consisted of: (1) day and hour cluster analyses of pay-toll data to define the OD matrices, including uncertainty characterization; (2) definition of the vehicles' population based on the regional registration data; and (3) other assumptions refer to the pay-toll queuing and features of driving behavior.

The simulations for the whole transportation network provided the trajectories of each vehicle on the network in the considered year. This information, in conjunction with finite-element structural models of the bridges, enabled the determination of the structural actions with distribution of maximum internal forces derived from traffic loads.

For three viaducts, the safety margin implied by the simulation-based structural assessment was compared with that following the application of conventional traffic loads recommended by the Eurocodes and current Italian

guidelines for bridge assessment. It was found that, in the considered case, the 1000-year return period flexural moments fell between 55% and 60% of the EN-1991-2 characteristic values, while the corresponding shear force maxima were between 50% and 70%.

The most noteworthy results of this study are the following: (i) the micro-simulations seem fit-for-purpose for structure-specific determination of traffic loads; (ii) the code-assigned loads tend to determine structural action safety margins significantly lower than the simulation-based counterpart; (iii) the traffic-induced loads are structure specific, and then the simulation of the entire network has been shown necessary. These results notwithstanding, two caveats also emerge: (iv) parties interested in following this approach should be aware that the calibration of the traffic model may be impaired by the availability of traffic flow data (or lack thereof) and is critical for the defensibility of the results; (v) traffic-induced actions with the desired return period, obtained as a low quantile of the fitted probability model, were larger than the maxima observed from simulated data by a factor of roughly two, indicating that longer time intervals may need to be simulated; (vi) the study neglected, only for simplicity, issues such as simulations of traffic accidents and the inertial effects of traffic loads on the bridges. It is ultimately believed that this study can contribute to the development of practical approaches for the safety assessment of transportation infrastructure.

ACKNOWLEDGMENT

This study was performed thanks to funding from the DiSt—Tangenziale di Napoli spa agreement of 2021. Any opinions or conclusions from the study do not necessarily reflect those of the funding entity.

REFERENCES

AASHTO. (2020). *AASHTO LRFD bridge design specifications*. American Association of State Highway and Transportation Official.

Adeli, H., & Ghosh-Dastidar, S. (2004). Mesoscopic-wavelet freeway work zone flow and congestion feature extraction model. *Journal of Transportation Engineering*, *130*, 94–103. https://doi.org/10.1061/(ASCE)0733-947X(2004)130:1(94)

Antoniou, C., Barceló, J., Breen, M., Bullejos, M., Casas, J., Cipriani, E., Ciuffo, B., Djukic, T., Hoogendoorn, S., Marzano, V., Montero, L., Nigro, M., Perarnau, J., Punzo, V., Toledo, T., & van Lint, H. (2016). Towards a generic benchmarking platform for origin–destination flows estimation/updating algorithms: Design, demonstration and validation. *Transport Research Part C: Emerging Technologies*, *66*, 79–98. https://doi.org/10.1016/j.trc.2015.08.009

Arora, P., Deepali, D., & Varshney, S. (2016). Analysis of K-Means and K-Medoids algorithm for big data. *Procedia Computer Science*, *78*, 507–512. https://doi.org/10.1016/J.PROCS.2016.02.095

ASCE/SEI 7 -22. (2022). *Minimum design loads and associated criteria for buildings and other structures*. https://doi.org/10.1061/9780784415788

Benjamin, J. R., & Cornell, C. A. (1970). *Probability, statistics, and decision for civil engineers*, McGraw-Hill, New York.

Buisson, C., Daamen, W., Punzo, V., Wagner, P., Montanino, M., & Ciuffo, B. (2014). Calibration and validation principles. In W. Daamen, C. Buisson, & S. P. Hoogendoorn (Eds.), *Traffic simulation and data* (pp. 105–134). CRC Press.

Caprani, C. C., OBrien, E. J., & Lipari, A. (2016). Long-span bridge traffic loading based on multi-lane traffic micro-simulation. *Engineering Structures*, *115*, 207–219. https://doi.org/10.1016/j.engstruct.2016.01.045

Cascetta, E., Punzo, V., & Montanino, M. (2011). Empirical analysis of effects of automated section speed enforcement system on traffic flow at freeway bottlenecks. *Transportation Research Record: Journal of the Transportation Research Board*, *2260*, 83–93. https://doi.org/10.3141/2260-10

Ciuffo, B., Punzo, V., & Montanino, M. (2012). Thirty years of Gipps' car-following model. *Transportation Research Record*, *2315*, 89–99. https://doi.org/10.3141/2315-10

Ciuffo, B., Punzo, V., & Torrieri, V. (2008). Comparison of simulation-based and model-based calibrations of traffic-flow microsimulation models. *Transportation Research Record: Journal of the Transportation Research Board*, *2088*, 36–44. https://doi.org/10.3141/2088-05

C.S.LL.PP. (2020). *Linee guida per la classificazione e gestione del rischio, la valutazione della sicurezza e il monitoraggio dei ponti esistenti*. Gazzetta Ufficiale della Repubblica Italiana.

C.S.LL.PP. (2018). *Norme tecniche per le costruzioni*. Gazzetta Ufficiale della Repubblica Italiana 42.

D.Lgs n.285/1992. (1992). *Nuovo Codice della Strada*. Gazzetta Ufficiale della Repubblica Italiana.

EN 1990. (2002). *Basis of structural design*. The European Union Per Regulation 305/2011, Directive 98/34/EC, Directive 2004/18/EC.

EN 1991-2. (2003). *Traffic loads on bridge*. The European Union Per Regulation 305/2011, Directive 98/34/EC, Directive 2004/18/EC.

Enright, B., Carey, C., & Caprani, C. C. (2013). Microsimulation evaluation of Eurocode load model for American long-span bridges. *Journal of Bridge Engineering*, *18*, 1252–1260. https://doi.org/10.1061/(ASCE)BE.1943-5592.0000546

Ghosh-Dastidar, S., & Adeli, H. (2006). Neural network-wavelet microsimulation model for delay and queue length estimation at freeway zones. *Journal of Transportation Engineering*, *132*, 331–341.

Grakovski, A., Yunusov, S., & Medvedev, A. (2020). Static approach for solving the problem of cargo weight distribution on vehicle's axles. In I. Kabashkin, I. Yatskiv, & O. Prentkovskis (Eds.), *Reliability and statistics in transportation and communication* (pp. 151–161). Springer.

Jiang, X., & Adeli, H. (2004). Wavelet packet-autocorrelation function method for traffic flow pattern analysis. *Computer-Aided Civil and Infrastructure Engineering*, *19*, 324–337. https://doi.org/10.1111/j.1467-8667.2004.00360.x

Karim, A., & Adeli, H. (2002). Incident detection algorithm using wavelet energy representation of traffic patterns. *Journal of Transportation Engineering*, *128*, 232–242. https://doi.org/10.1061/(ASCE)0733-947X(2002)128:3(232)

Lipari, A., Obrien, E., & Caprani, C. (2012). A comparative study of bridge traffic load effect using micro-simulation and

Eurocode load models. In *Bridge Maintenance, Safety, Management, Resilience & Sustainability* (pp. 3420–3427). Stresa, Italy.

Lu, Q., Harvey, J., Lea, T., Lea, J., Quinley, R., Redo, D., & Avis, J. (2002). *Truck traffic analysis using weigh-in-motion (WIM) data in California*. University of California, Berkeley, Institute of Transportation Studies Pavement Research Center.

Jin, X., & Han, J. (2011). K-Medoids clustering. In C. Sammut, & G. I. Webb (Eds.), *Encyclopedia of machine learning* (pp. 564–565). Springer US.

Mathieu, H., Calgaro, J. A., & Prat, M. (1991). *Concerning development of models of traffic loading and rules for the specification of bridge loads*. Final Reports to the Commission of the European communities on Contract PRS/89/7750/MI/15 and PRS/90/7750/RN/46.

Menn, C. (1990). *Prestressed concrete bridges*. Springer.

O'Brien, E. J., Schmidt, F., Hajializadeh, D., Zhou, X.-Y., Enright, B., Caprani, C. C., Wilson, S., & Sheils, E. (2015). A review of probabilistic methods of assessment of load effects in bridges. *Structural Safety*, *53*, 44–56. https://doi.org/10.1016/j.strusafe.2015.01.002

Olstam, J., & Tapani, A. (2011). A review of guidelines for applying traffic simulation to level-of-service analysis. *Procedia Social and Behavioral Sciences*, *16*, 771–780. https://doi.org/10.1016/j.sbspro.2011.04.496

Punzo, V., Ciuffo, B., & Montanino, M. (2012). Can results of car-following model calibration based on trajectory data be trusted? *Transportation Research Record*, *2315*(10), 11–24. https://doi.org/10.3141/2315-02

Punzo, V., Ciuffo, B., & Montanino, M. (2014). Sensitivity analysis. In C. Buisson, S. P. Hoogendoorn, & W. Daamen (Eds.), *Traffic simulation and data: Validation methods and applications* (pp. 119–139). CRC Press.

Punzo, V., & Montanino, M. (2020). A two-level probabilistic approach for validation of stochastic traffic simulations: Impact of drivers' heterogeneity models. *Transport Research Part C: Emerging Technologies*, *121*, 102843. https://doi.org/10.1016/j.trc.2020.102843

Rafati Fard, M., & Shariat Mohaymany, A. (2019). A copula-based estimation of distribution algorithm for calibration of microscopic traffic models. *Transport Research Part C: Emerging Technologies*, *98*, 449–470. https://doi.org/10.1016/j.trc.2018.12.008

Sirca, G. F., & Adeli, H. (2005). Case-based reasoning for converting working stress design-based bridge ratings to load factor design-based ratings. *Journal of Bridge Engineering*, *10*, 450–459. https://doi.org/10.1061/(asce)1084-0702(2005)10:4(450)

Treiber, M., Kesting, A., & Wilson, R. E. (2011). Reconstructing the traffic state by fusion of heterogeneous data. *Computer-Aided Civil and Infrastructure Engineering*, *26*, 408–419. https://doi.org/10.1111/j.1467-8667.2010.00698.x

Ugray, Z., Lasdon, L., Plummer, J. C., Glover, F., Kelly, J., & Martí, R. (2005). A multistart scatter search heuristic for smooth NLP and MINLP problems. In C. Rego & B. Alidaee (Eds.), *Metaheuristic optimization via memory and evolution* (pp. 25–57). Kluwer Academic Publishers.

Waheed, A., & Adeli, H. (2000). A knowledge-based system for evaluation of superload permit applications. *Expert Systems with Applications*, *18*, 51–58. https://doi.org/10.1016/S0957-4174(99)00050-0

Wiśniewski, D. F., Casas, J. R., & Ghosn, M. (2012). Codes for safety assessment of existing bridges—current state and further development. *Structural Engineering International*, *22*, 552–561. https://doi.org/10.2749/101686612x13363929517857

Zhang, B., Zhou, L., & Zhang, J. (2019). A methodology for obtaining spatiotemporal information of the vehicles on bridges based on computer vision. *Computer-Aided Civil and Infrastructure Engineering*, *34*, 471–487. https://doi.org/10.1111/mice.12434

How to cite this article: Testa, G., Zaccaria, G., Montanino, M., Baltzopoulos, G., Bilotta, A., Iervolino, I., & Punzo, V. (2023). Infrastructure-level traffic micro-simulation for probabilistic analysis of bridge loads. *Computer-Aided Civil and Infrastructure Engineering*, *38,* 1217–1235. https://doi.org/10.1111/mice.12950